AIAA 80-0771R

Wind-Tunnel Investigation of Active Controls Technology Applied to a DC-10 Derivative

B.A. Winther,* W.A. Shirley,† and R.M. Heimbaugh‡
Douglas Aircraft Company, Long Beach, Calif.

Application of active controls technology to reduce aeroelastic response offers a potential for significant payoffs in terms of aerodynamic efficiency and structural weight. As part of the Energy Efficient Transport program, the impact on flutter and gust load characteristics has been investigated by means of analysis and low-speed wind tunnel tests of a semispan model. The model represents a DC-10 derivative with increased wingspan and an active aileron surface, responding to vertical acceleration at the wingtip. A control law satisfying both flutter and gust load constraints is presented and evaluated. In general, the beneficial effects predicted by analysis are in good agreement with experimental data.

Nomenclature

a,b,c	= coefficients of aerodynamic approximation
$A(k)$	= aerodynamic generalized force
C	= eigenvalue matrix
d_A	= rotational damping of actuator
$f_n(t)$	= input force
$F(t),G(t)$	= matrices containing input forcing function
g	= modal damping
G_p	= transfer function of phase filter
G_s	= transfer function of actuator servo
H_A	= transfer function of valve/actuator
j_p	= polarity of phase filter
k	= reduced frequency
k_A	= rotational stiffness of actuator
M,D,K	= matrices containing generalized forces due to structural and aerodynamic inertia, damping, and stiffness
$\ddot{h}_{WT}$	= wing acceleration
$\ddot{\ell}_E$	= engine lateral acceleration
N	= number of modes
n	= mode number
p,q	= generalized coordinates
s	= Laplace variable
t	= time
V_D	= design dive speed
δ	= control surface deflection
ϕ	= phase angle
τ	= time constant
ω	= circular frequency

Introduction

THE rising price of fuel has dramatically increased operating costs for commercial transports. Until the 1973 oil embargo, the price of fuel accounted for only a modest portion of the direct operating costs (DOC) of transport aircraft. Five years later, however, the fuel fraction of DOC had nearly doubled—from 24 to 40% (Fig. 1). Today this figure is closer to 50%. One-half of the airlines' DOC are spent for fuel and oil!

Presented as Paper 80-0771 at the AIAA/ASME/ASCE/AHS 21st Structures, Structural Dynamics and Materials Conference, Seattle, Wash., May 12-14, 1980; submitted June 10, 1980; revision received Jan. 16, 1981.

*Principal Engineer, Dynamics Group. Member AIAA.
†Task Manager, Active Controls, Energy Efficient Transport.
‡Senior Engineer, Flight Dynamics Group.

Aircraft design of the 1980's must take into account these spiraling fuel costs. We can no longer rely on the performance and profit ratios established in the 1960's and 1970's. Fuel efficiency is a crucial factor in the design of both new and derivative aircraft.

One of the technologies being developed to improve fuel efficiency is active controls. Reduced drag and lower structural weight can be realized by using control surfaces for static stabilization and load alleviation functions. Once the aircraft controls are designed for multiple use and high response, it is but a small additional step to utilize them in flutter margin augmentation, which provides additional weight savings for many aircraft. These controls also facilitate the economic incorporation of other advanced aerodynamic features. Winglets and supercritical wings, for example, have already promised better aerodynamic efficiency. Our analysis has shown that these features may result in a flutter critical design which must absorb a structural weight increment or rely on augmentation to stabilize the flutter modes.

The authors' company is currently participating in the Aircraft Energy Efficiency Program (ACEE). A portion of this program is designed to accelerate technology development in advanced aerodynamics and active controls. Douglas has designed, built, and tested a model of a derivative DC-10 with active gust load alleviation and flutter suppression. This paper reports on the results of analysis and testing of the model in the Douglas low-speed wind tunnel at Long Beach.

Design Considerations

The wind tunnel model is designed as a semispan wing, representative of a DC-10 derivative airplane with an aspect ratio of 8.56, a taper ratio of 0.192, and a quarter-chord sweep of 35 deg. One important objective of the test is to confirm existing analysis methods for dynamic loads and flutter stability and to explore use of the control system to suppress critical modes at speeds above the design dive speed V_D. Future applications of active control systems will probably be certified within existing commercial aircraft criteria.[1] These criteria require the aircraft to be free of flutter up to 1.2 V_D. In addition, the aircraft must be free of flutter at any speed up to V_D after certain failures, including failures of automatic flight control systems. Near-term application of active control systems is likely to provide flutter margin augmentation, such that the flutter speed is increased from V_D (or higher) with the system inoperative to 1.2 V_D (or higher) with the system. Under these circumstances, the criteria for certification can be met with a failed system. For active control systems, such as the system described herein, the probability of system failure normally would fall within the "probable" range (greater than 10^{-5} per flight hour).[2]

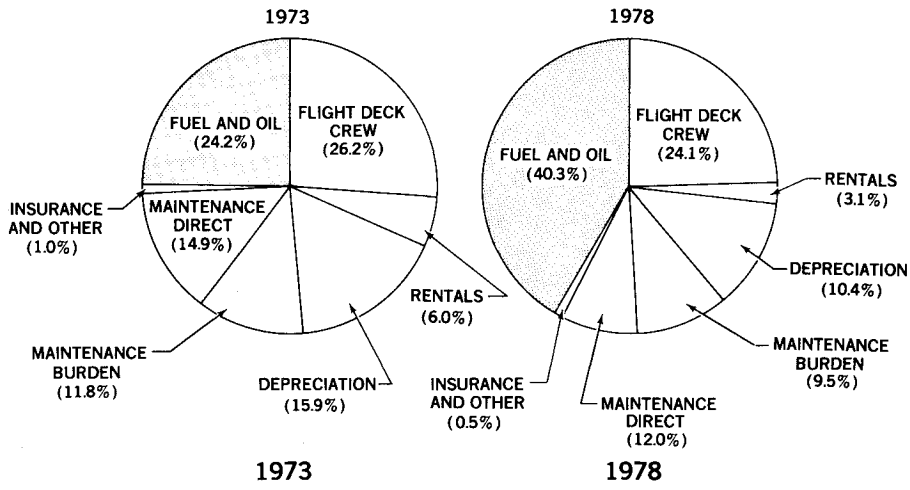

Fig. 1 Direct operating cost relationship for domestic U.S. trunk airlines.

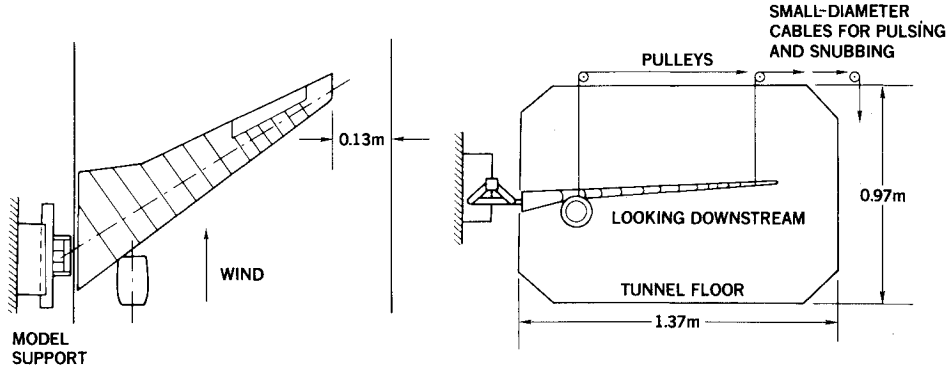

Fig. 2 Installation of model in the wind tunnel.

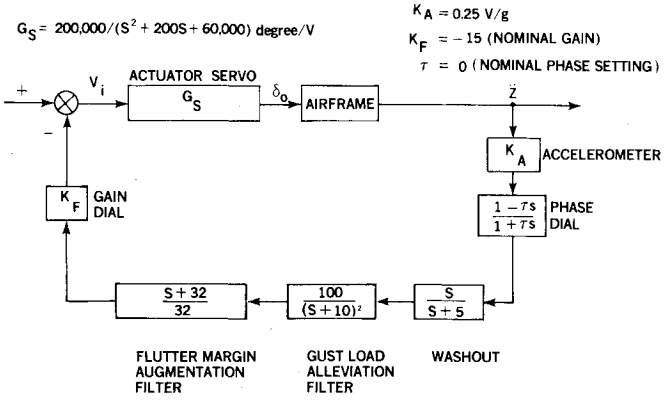

Fig. 3 Active control system.

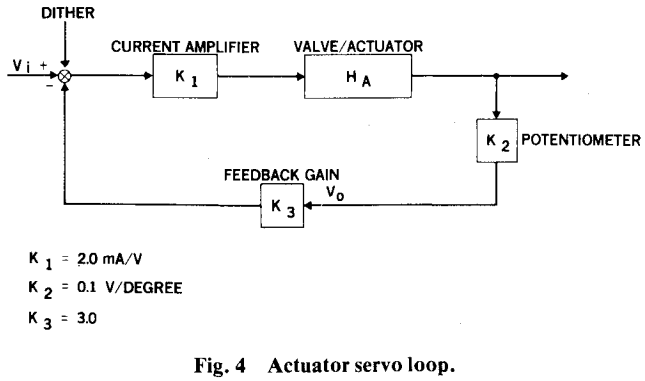

Fig. 4 Actuator servo loop.

The goal was to provide a 20% flutter margin augmentation and a 30% reduction of the critical wing bending moment due to turbulence.

Model Design

The aeroelastic modeling of the wing (Fig. 2) consisted of 16 balsa wood segments attached to a solid aluminum spar. The engine was represented by a flow-through nacelle attached to a beam simulating the important pylon degrees of freedom required to provide correct structural coupling for flutter. Design scale factors were selected to fit the model into the Douglas Long Beach Wind Tunnel, which has a rectangular test section (0.97 × 1.37 m) and an operational speed limit of 67 m/s. Small-diameter cables attached to the nacelle and the wing tip were used to pulse the model and to suppress any instabilities that occurred during flutter testing.

The outboard aileron, powered by a rotary hydraulic actuator, was designed to provide flutter suppression and load reduction in turbulence. The control surface was made of balsa wood covered with aluminum skin for strength. Aluminum fittings were used to support three steel bearings along the hinge line. A potentiometer measuring aileron deflection (maximum ±15 deg) was connected to the actuator shaft. At three locations along the wing spar, strain gages were mounted to sense wing bending and torsion. Accelerometers were located in the nacelle to sense both vertical and lateral acceleration. The feedback signal for the active system was supplied by an accelerometer installed near the wing tip. Each transducer output was amplified by a signal conditioning unit which delivered the signal to a direct-write oscillograph, a tape recorder, and an analog computer for further processing. The control law implemented on the computer is presented in Fig. 3.

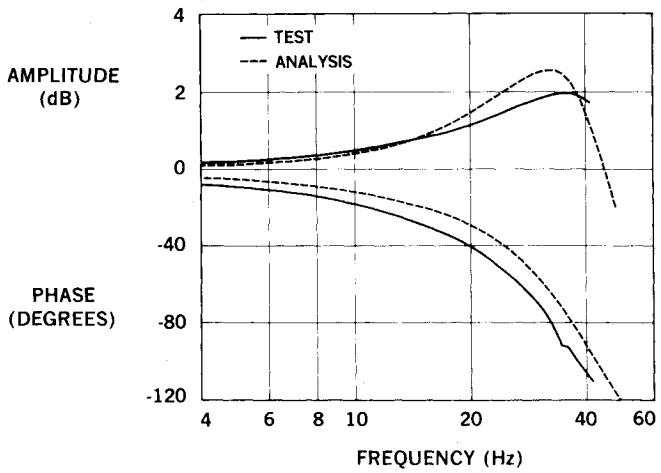

Fig. 5 Measured and computed transfer function of the actuator servo.

Actuator Servo Design

The actuator servo was designed with simple position feedback, as illustrated by the block diagram in Fig. 4. In order to reduce the effect of friction in the servovalve, a dither signal (360 mV, 400 Hz) was supplied to the current amplifier. Functional checks of the actuator and other components in the control system were first made in a bench test and later in the model with the system installed. With a spring mounted on the actuator shaft to simulate the aerodynamic load, the position feedback gain was determined so that the servo had a 6 dB margin. The transfer function of the valve/actuator was approximated by

$$H_A = \frac{10^5}{s(s+200)} \text{ deg/mA}$$

With a current amplifier gain of 2.0 mA/V, potentiometer sensitivity of 0.1 V/deg, and a feedback gain of 3.0, the transfer function of the actuator servo becomes

$$G_S = \frac{200{,}000}{s^2+200s+60{,}000} \text{ deg/V}$$

Tests were performed to measure the servo output vs input command.

Figure 5 shows a comparison between the measured transfer function and this equation.

Analytical Procedure

We have represented structural displacements in the conventional manner by using a linear combination of selected displacement functions, each of which is associated with a time-dependent generalized coordinate q_n. The displacement functions are chosen from a limited number of low-frequency natural vibration modes of the structure. The control surface rotation is included in the set as the last displacement function with a corresponding generalized coordinate q_N represented by the angular deflection $\delta(t)$. All displacements are assumed to be small so that elastic restoring forces in the structure can be approximated by linear combinations of linear operators acting on the displacement functions. A similar linearization is applied to the resulting aerodynamic forces. Considering equilibrium of the generalized forces derived from Lagrange's equation, a system of linear differential equations is obtained. All coefficients with the exception of aerodynamic terms in the equations are independent of time and flight condition.

The dynamic response to input forces $f_n(t)$ is computed by solving the system of linear equations. If the input force is supplied by control surface commands, the function $f_n(t)$ becomes

$$f_n(t) = \begin{cases} 0 & \text{for } n=1,2,\ldots(N-1) \\ k_A\delta + d_A\dot{\delta} & \text{for } n=N \end{cases}$$

where k_A and d_A represent the rotational stiffness and damping of the actuator. The dynamic equations are solved with the assumption that the input functions are harmonic. Atmospheric turbulence is also represented by harmonic components which are assumed to be random in nature.

For analysis of flutter stability, the input function is eliminated and the problem is reformulated by requiring a match between the eigenvalue solution and the reduced frequency of the aerodynamic terms. The flutter speed is obtained when the total system damping g goes to zero. The total damping includes the structural damping which is determined by ground vibration tests.

The procedures described above have been used to compute the dynamic response and flutter stability both with and without the effects contributed by the active control system. For control system synthesis, however, it is necessary to directly obtain the aeroelastic transfer functions in an explicit form. To meet this requirement, the equations of motion are simplified by introducing a frequency-domain approximation of the aerodynamic coefficients $A(k)$ in the form

$$A(k)q(t) = a\dot{q}(t) + bq(t) + c\ddot{q}(t)$$

where a, b, and c are real coefficients dependent upon the reduced frequency. The approximation is made piecemeal by use of the functional values of $A(k)$ at $k=0$ and a k value in the neighborhood of a chosen reduced frequency k_1. The coefficients used to approximate the aerodynamic forces are combined with the generalized forces due to structural mass, damping, and stiffness into a set of equations that is expressed in matrix form by

$$M\ddot{q} + D\dot{q} + Kq = F(t)$$

The eigenvalues and eigenvectors of the homogeneous equation are computed in an iterative manner by letting k_1 assume the reduced-frequency value k_n obtained in the preceding iteration for root number n. Using the resulting eigenvectors, the generalized coordinates q are transformed into a new set of generalized coordinates associated with the uncoupled equations of motion. With the eigenvalues known, the transformed equations are reduced into a first-order form similar to the equation[3]

$$\dot{p} = Cp + G(t)$$

where C is an eigenvalue matrix. This equation is in a form compatible with existing control system analysis routines.

The control system analysis considers 12 generalized degrees of freedom. This size reduction is achieved by truncating the original structural degrees of freedom in a manner that retains the residual effects of higher-order modes. To reduce the control system design process even further, the equations of motion described above has been developed for only a limited number of configurations and flight conditions.

The following procedures were used to develop the control law: 1) the linear-differential equations described above were used to compute transfer functions relating accelerometer and load responses to aileron and gust inputs; 2) classical control theory techniques were used to design a control law to perform the flutter suppression and gust load alleviation functions; 3) the control law performance was verified by conducting closed-loop frequency domain flutter and gust analyses; and 4) the control law was modified, as necessary, to improve performance.

Table 1 Measured and computed frequencies of the natural modes for two fuel configurations

	Frequency, Hz			
	0% Fuel		100% Fuel	
	Test	Analysis	Test	Analysis
1st wing bending	5.29	5.23	3.61	3.57
Engine yaw	6.28	6.23	6.27	623
Engine pitch/wing torsion	12.50	12.52	12.47	12.53
2nd wing bending	16.33	16.31	10.77	11.03
Engine roll	23.07	23.13	23.69	23.44
Wing fore and aft bending	23.27	23.25	15.68	15.58
3rd wing bending	34.73	33.19	22.65	21.87
2nd wing torsion	42.26	40.68	33.93	31.26

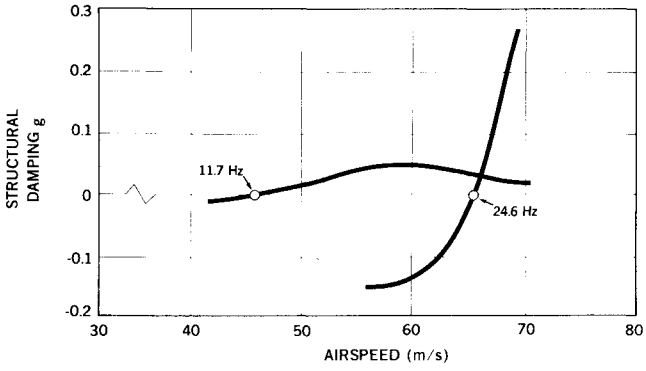

Fig. 6 Computed flutter characteristics.

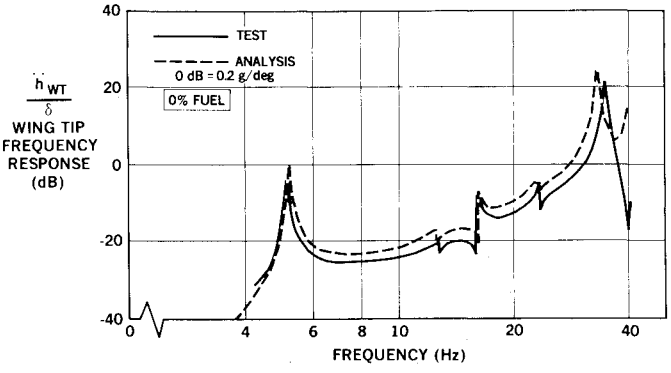

Fig. 7 Measured and predicted wingtip acceleration due to aileron input at zero airspeed.

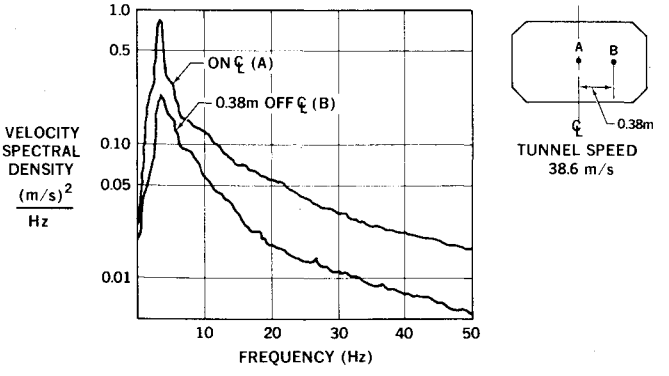

Fig. 8 Measured power spectrum density of the vertical velocity with banner installed.

Test Procedure

To realistically demonstrate the performance of the gust load alleviation and flutter margin augmentation systems, critical bending moments and airspeeds were identified by analysis prior to the model design phase. The wing bending moment response due to turbulence was found to be most significant near the middle of the wingspan. At inboard locations, the design was determined on the basis of maneuver loads. Near the wingtip, minimum gage constraints were predominant.

Based on preliminary analysis, the most critical bending moment due to turbulence was predicted for 100% wing fuel. The most critical flutter configuration, however, was obtained for 0% fuel loading. Consequently, these two configurations were selected for detailed and wind-tunnel testing. Figure 6 presents the computed flutter characteristics for the two modes of interest at 0% wing fuel. The critical mode contains essentially engine pitch and first wing torsion. This mode is lightly damped throughout the normal speed range and displays a typical "hump" damping characteristic. The second mode containing second wing torsion is stable up to relatively high speed.

The wind tunnel activity was preceded by a comprehensive ground test program to verify and improve the analytical representation and the derived control laws.

Ground Test

Structural properties of the model were validated through a conventional ground vibration test using a shaker to excite the natural modes of the model. The test was completed for the empty- and full-wing fuel conditions with the aileron held fixed. A comparison of measured and predicted frequencies is presented in Table 1. Later, during the wind tunnel program, vibration testing was repeated occasionally to verify the structural integrity of the model.

Interaction between the structure and the active control system was validated by measuring the open-loop model response to aileron input. The measured frequency response of the vertical acceleration at the wing tip is presented in Fig. 7 together with results predicted by analysis. To explore possible resonance conditions with the active control loop closed, intermittent pulses were applied to the wingtip and the engine for varying values of the loop gain. As a result of these tests, feedback gain was lowered somewhat to retain desired stability margins for the zero airspeed condition. Note in Figs. 7, 14, and 15 that the amplitudes of the transfer functions at the reference 0 dB level are not "one," but rather the values noted in each figure.

Wind Tunnel Test

The model was tested in the Douglas Long Beach Wind Tunnel. Artificial turbulence for investigation of gust loads was generated by a fabric banner (0.3-m wide) installed horizontally across the tunnel at a station approximately 5 m

upstream of the test section. Prior to model installation, the vertical velocity component created by the banner was measured for three different speeds at three positions across the test section. The power spectral density of the velocity is presented in Fig. 8 for a tunnel velocity of 38.6 m/s. It was observed that the intensity of the turbulence was substantially higher at the center of the test section than at locations closer to the walls. Furthermore, the shape of the power spectrum was observed to differ substantially from the spectra generally used to describe atmospheric turbulence. The slope of the spectrum at high frequency was estimated to be −14 dB/decade, compared to −20 dB/decade for the Dryden spectrum.[4] To analytically predict the model response due to turbulence, an approximation of the measured spectrum was used. The intensity of the turbulence was represented by a parabolic approximation having zero velocity near the tunnel wall.

In the initial phase of the model test, a primary objective was to explore the open-loop characteristics. With the banner installed in the tunnel to generate a near-random gust field, the aeroelastic response of the model was measured in terms of wing bending and torsional moments (at three spanwise locations), vertical and lateral engine accelerations, aileron position, and wing tip vertical acceleration. The data were processed on a real-time spectrum analyzer. This procedure allowed the test engineer to rapidly evaluate the performance by comparing the spectra obtained with and without the control system in operation. Some data were recorded on magnetic tape for detailed processing at a later time. The gust response test was performed at several speeds below the passive flutter speed with variations in gain and phase of the active system. Phase variations were obtained by inserting a filter

$$G_p = j_p\left(\frac{1-\tau s}{1+\tau s}\right) \qquad \begin{cases} j_p = -1 & \text{for phase lag} \\ j_p = -1 & \text{for phase lead} \end{cases}$$

in the control loop. The time constant τ for a given phase angle ϕ (in degrees) at frequency ω was determined by

$$\tau = \tan[(1-j_p)45 - \phi/2]/\omega$$

where ϕ is plus for phase lead.

The open- and closed-loop flutter characteristics were determined by monitoring subcritical response to pulse input. The interaction between the aeroelastic system and the control system was explored by measuring the frequency response due to aileron excitation both above and below the passive flutter speed. The banner was not used during these tests. Gain and phase variations were conducted in the same manner as in the gust response test.

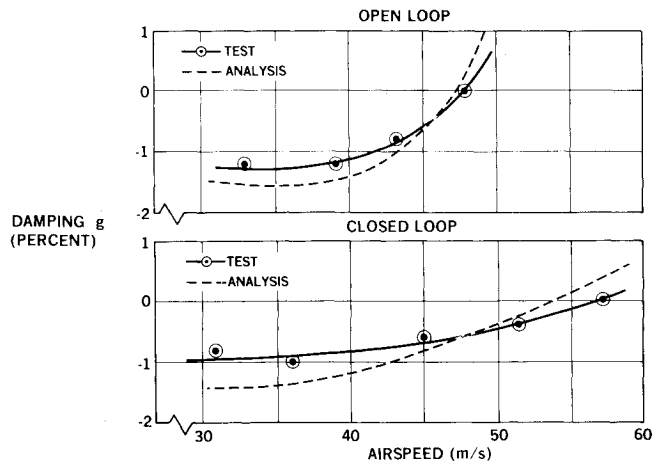

Fig. 9 Open- and closed-loop flutter characteristics for the zero-fuel configuration.

Discussion of Test Results

The purpose of the initial test was to investigate a simple feedback system. Since the model was cantilevered at the tunnel wall, the first wing mode was predominant in the bending moment response caused by turbulence. Therefore, the control system, designed for alleviation of the bending moment, employed one single accelerometer located close to the wing tip where the acceleration response of the first wing mode was most significant.

During the early stages of the program, it became clear that evaluation of the test data, obtained in the first tunnel entry, would lead to improvements in the control law. For this reason, continued testing with the existing semispan model was scheduled. Furthermore, in order to evaluate a complete airplane configuration having all of the rigid-body degrees of freedom, another test (with a more complex control system) was also scheduled. For this test, provisions were made so that the existing semispan model will be used again as the left-hand side of the complete aircraft model, which will then be equipped with both active elevator and aileron surfaces.

The data reported herein were obtained from wind tunnel tests of the semispan model.

Flutter Stability

The flutter characteristics of the model result primarily from dynamic interaction between fundamental wing bending and a mode consisting of engine pitch and wing torsion. The natural frequency of the wing bending mode depends on fuel loading. At zero airspeed, the natural frequency (even with zero fuel) is well below the response frequency of the engine pitch mode. With increasing airspeed, the frequency of the bending response approaches the engine pitch frequency. At some airspeed the two modes coalesce, resulting in a loss of damping. The instability is relatively mild as illustrated by Fig. 9. For zero fuel, the measured flutter speed is 47.9 m/s at the nominal structure damping. Increasing the structural damping from its nominal value 0.88 to 1.4% by adding damping material to the engine pylon results in a flutter speed of 49.4 m/s.

With the active control loop closed the flutter speed is increased by 19% to 57.1 m/s. At higher fuel loadings, the effect of the active system is reversed, as illustrated by Fig. 10. The flutter characteristics of the zero fuel configuration are sensitive also to gain and phase variation in the control law.

At high-gain values, the third wing bending mode is driven unstable below the passive flutter speed (Fig. 11). Figure 12 presents the effects of phase variations as provided by the phase dial network at the approximate flutter frequency, 12 Hz. The analytically predicted flutter speed for nominal gain is 5% lower than demonstrated in the test. The flutter boundary for the third wing bending mode (35 Hz) is predicted to within 7-10% of the test data. The accuracy is determined primarily by differences in the structural

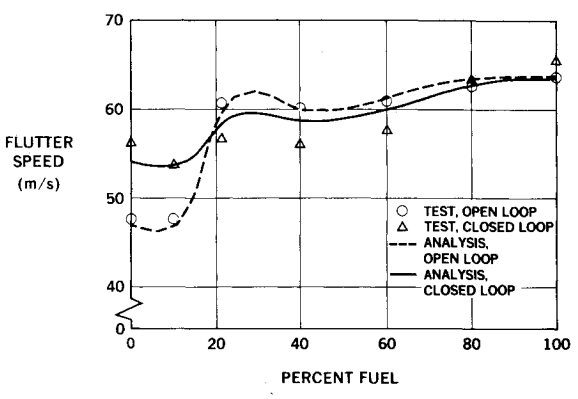

Fig. 10 Flutter speed vs fuel.

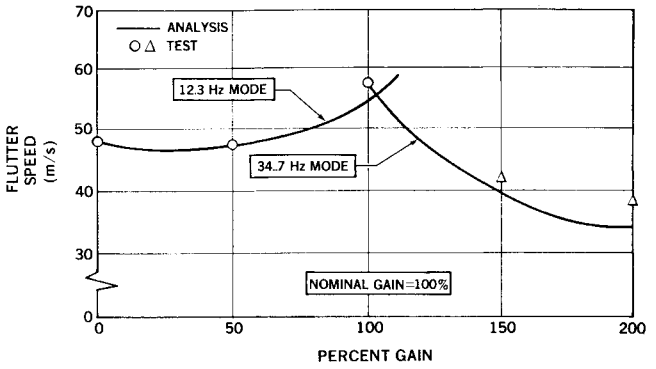

Fig. 11 Flutter speed vs gain for zero-fuel configuration.

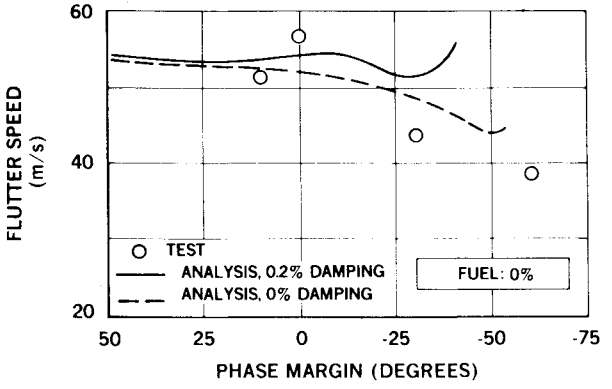

Fig. 12 Phase margin of the 12-Hz mode.

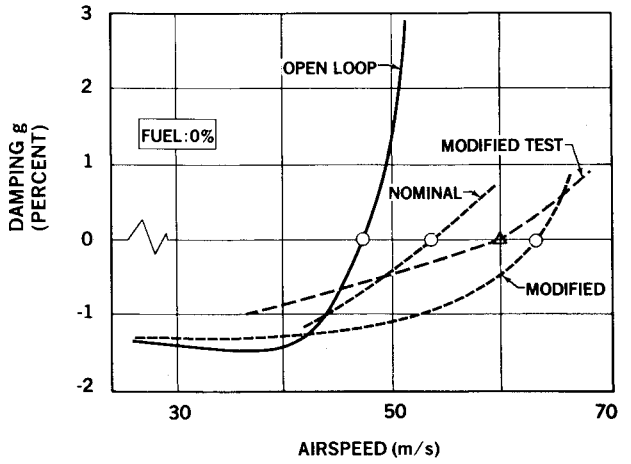

Fig. 13 Computed flutter characteristics with modified control law.

representation. Recent analysis has shown that the third wing bending mode is stabilized by placing the feedback accelerometer further inboard on the wing. The stabilization of this mode allows an increase in the feedback gain and a substantial increase in the flutter speed. Subsequent test data verified this prediction as shown in Fig. 13.

Dynamic Response

The dynamic loads investigated during the test are caused either by control surface motion or by the generated turbulence in the wind tunnel. The bulk of these measurements relates to the full-fuel configuration. Figures 14 and 15 present magnitudes of the wing tip acceleration and the engine lateral acceleration due to aileron excitation. The analytical data reflect correction factors applied to the theoretically computed aileron forces which typically are 40% higher than

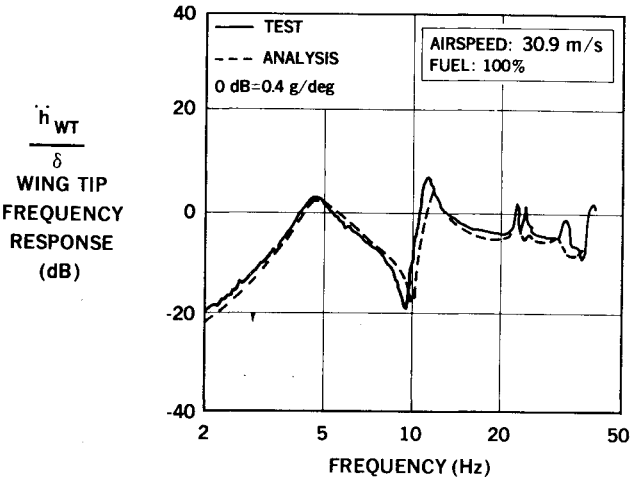

Fig. 14 Wingtip acceleration per degree of aileron excitation.

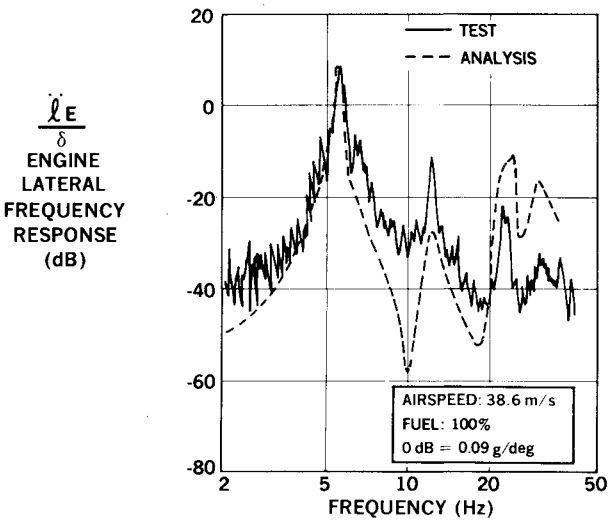

Fig. 15 Frequency response of engine lateral acceleration due to control surface excitation.

measured quantities. With correction factors based upon aerodynamic test data for steady flow, the response due to aileron motion is predicted with good accuracy.

In developing an effective gust load alleviation system, the initial analyses were based on the assumption that the model would be tested in a gust environment similar to atmospheric turbulence. As discussed earlier, both the spanwise distribution of the gust intensity and the spectral shape of the flowfield were found to differ from natural turbulence. In subsequent analyses, the flowfield was considered to be spanwise uncorrelated and to have an intensity represented by the parabolic approximation.

These assumptions provide good agreement between measured and predicted data, even though the analysis tends to underestimate the response in some cases. Therefore, it appears that the generated turbulence is essentially uncorrelated. This assumption, however, should be verified by further testing. Figure 16 shows comparisons between measured and computed bending moments with the control loop open and closed. As demonstrated by Fig. 17, the predicted bending moment reduction due to the active system is generally less than that actually obtained in the test. This discrepancy in load reduction is explained by the analytical underestimation of wing tip acceleration and by the resulting control surface response. The active system produced no change in the measured midspan torque. The midspan torque (49% span) was measured at a tunnel speed of 30.9 m/s.

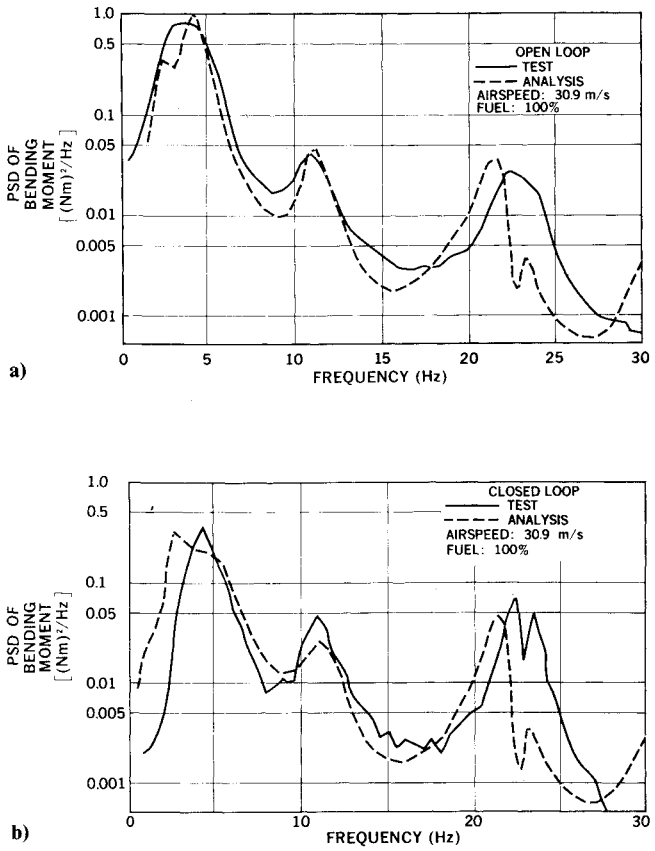

Fig. 16 Power spectrum density of 49% span bending moment due to turbulence: a) open-loop, b) closed-loop.

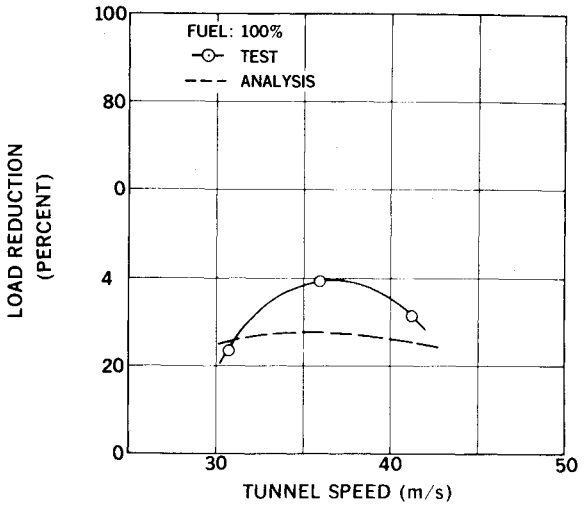

Fig. 17 Reduction of rms bending moment at 49% span.

Concluding Remarks

The beneficial effects predicted by analysis were verified by experiment. The active control system generated an increase in flutter speed for light fuel loadings, a decrease in flutter speed for intermediate fuel loadings, and a slight increase in flutter speed for the heaviest fuel configurations. Flutter speed margin for the most critical fuel configuration was raised by 15%. Gain and phase margins were found to be less than desired. In addition, the control system was found to reduce the subcritical damping of the model. Recent analysis and testing have indicated that these characteristics can be improved by relocation of the acceleration feedback sensor. Two or more alternate control laws will be explored when the wind tunnel test resumes.

The gust load alleviation system was very effective in reducing the overall wing bending moment response, particularly the contribution of the first wing bending mode to the total response. Measured values of the critical bending moment relief varied from 23% up to 40%. Loads due to the generated turbulence were predicted reasonably well by assuming that the gust field was spanwise uncorrelated.

Construction of the model involved development of a miniature hydraulic actuator and its associated servo components. The equipment functioned as expected during the major portion of the test program, but repairs proved to be time-consuming. It is desirable to improve the reliability of the system prior to development of the more complex systems to be installed in a full-span model later this year. New seal materials for the actuator vane and replacement of the potentiometer in the actuator servo by a linear variable differential transformer (LVDT) are being considered as reliability improvement.

Acknowledgments

The work presented in this paper was performed at Douglas Aircraft Company under NASA Contract NAS1-15327-02. Contributions from several individuals with the Dynamics, Loads, Avionics, and Mechanical Engineering Groups at Douglas are acknowledged.

References

[1] "Airworthiness Standards: Transport Category Airplanes," Federal Aviation Regulation, Pt. 25, Department of Transportation, Federal Aviation Administration, June 1974.

[2] Treacy, J.J., "The Use of Probability Analysis in Aircraft Certification and Its Effects on Maintenance and Equipment Maintenance," AIAA Paper 77-1256, Aug. 1977.

[3] Halfman, R.L., *Dynamics,* Vol. II, Addison-Wesley, Reading, Mass., pp. 392-433.

[4] "Flying Qualities of Piloted Airplanes, MIL-F-8785B (ASG), Aug. 7, 1969.